ELSEVIER

Chemistry & Biology 8 (2001) 967–980

Chemistry & Biology

www.elsevier.com/locate/chembiol

Research Paper

DNA bending by asymmetrically tethered cations: influence of tether flexibility

Philip R. Hardwidge [a], Dong-Kye Lee [b], Thazha P. Prakash [b], Beatriz Iglesias [b], Robert B. Den [a], Christopher Switzer [b,1], L. James Maher III [a,*]

[a] *Department of Biochemistry and Molecular Biology, Mayo Foundation, Rochester, MN 55905, USA*
[b] *Department of Chemistry, University of California at Riverside, Riverside, CA 92521, USA*

Received 26 March 2001; revisions requested 22 May 2001; revisions received 14 June 2001; accepted 19 June 2001
First published online 13 August 2001

Abstract

Background: We have been studying the proposal that laterally asymmetric charge neutralization along the DNA double helix can induce collapse toward the neutralized surface. Results of previous experiments implied that such a phenomenon can occur, suggesting a role for local interphosphate repulsive forces in DNA shape and rigidity.

Results: We now show that, whereas six ammonium ions tethered to one DNA face on flexible propyl chains can induce detectable DNA curvature, tethering of ammonium ions on rigid propynyl tethers does not induce DNA curvature. Molecular modeling indicates differing propensities for phosphate salt bridge formation between propyl- and propynyl-tethered ammonium ions.

Conclusions: Ammonium ion localization is suggested as a key factor in induced bending. Rigidification of the double helix by stacking of propyne groups cannot be excluded.

Keywords: DNA bending; DNA curvature; Electrophoresis; Cations; Asymmetric neutralization; Phosphate; Base analogs

1. Introduction

Although often considered to be a locally linear molecule, the DNA double helix commonly adopts sequence-dependent curved conformations and can be bent by proteins [1]. DNA segments shorter than 150 bp are, on average, energetically constrained from substantial curvature, behaving more like stiff rods with elastic resilience [1]. Conventional reasoning suggests that two classes of forces act to perturb the canonical double helical geometry of DNA. Intrinsic forces (base stacking, hydrogen bonding, and van der Waals interactions) result in the spontaneous deformation of some DNA sequences, resulting in DNA curvature. Extrinsic forces, resulting from the binding of proteins, drugs, and ions, can also change the shape of DNA. These induced deformations are termed DNA bending.

The energetic cost of DNA bending can be paid by the combination of thermal energy and favorable, non-covalent interactions with ligands. Thus, ligand binding can drive the bending of relatively short, rod-like DNA segments into compact, folded nucleoprotein structures. Such DNA shape alterations are important to DNA replication [2], transcriptional regulation in prokaryotes [3] and eukaryotes [4], and the packaging of DNA into nucleosomes [5].

Two general motifs are recognized among DNA bending proteins [6]. Class I DNA bending proteins (e.g. TATA binding protein and high mobility group proteins) interact with the DNA through the intercalation of hydrophobic amino acids between base pairs in the DNA minor groove, causing DNA bending away from the bound protein [7,8]. Class II DNA bending proteins (e.g. CAP and the histone octamer) interact with the DNA through multiple contacts including ionic interactions between cationic amino acids and the DNA sugar-phosphate backbone [4,5], causing DNA bending toward the bound protein.

In his formulation of quantitative models for electro-

[1] Also corresponding author.

* Corresponding author.
E-mail addresses: switzer@mail.ucr.edu (C. Switzer), maher@mayo.edu (L.J. Maher III).

1074-5521/01/$ – see front matter
PII: S1074-5521(01)00065-5

static effects in DNA curvature and bending, Manning conceived of local DNA shape as reflecting an equilibrium between opposing forces of compression (e.g. base stacking, van der Waals contacts) and stretching (e.g. interphosphate Coulombic repulsion) [9,10]. In this view, the balance between compression and stretching forces contributes to DNA rigidity and local shape. Manning reasoned that stretch forces are dominated by local interphosphate repulsions, because physiological salt concentrations efficiently screen longer range charge–charge interactions. It was then reasoned that asymmetries in stretching forces along different DNA faces could arise from irregularities in phosphate neutralization by counterions or proteins. Calculations suggested that modest asymmetries in residual phosphate charge could induce significant DNA curvature due to unbalanced stretching forces [10].

This neutralization–collapse model predicts that the approach of a cationic protein to the DNA backbone effectively cancels local phosphate charges, leading to an asymmetric decrease in phosphate–phosphate charge repulsions on the protein-bound face of the helix. Because condensed monovalent cations are thought to neutralize about 80% of DNA phosphate charge, whereas salt bridges may effectively neutralize 100% of the charge of certain phosphates, the resulting unbalanced interphosphate repulsions are predicted to generate forces that tend to cause a collapse of the DNA backbone towards the protein [9,10]. Important contributions to DNA bending undoubtedly also result from mutual accommodation at the protein/DNA interface (driven by van der Waals forces and by entropically favored displacement of counterions). Our laboratories have focused on whether neutralization–collapse of the DNA backbone plays a significant role in DNA bending by proteins [11–14].

Recently it has been suggested that the neutralization–collapse model should be extended to understanding intrinsic DNA curvature. Williams and co-workers [15,16] and Hud and Feigon [17,18] argue that asymmetries in counterion distributions in the DNA grooves may be important in determining intrinsic DNA geometry, raising the possibility that the electrostatic effects of ion distributions are at least as important as base stacking interactions in determining sequence-dependent DNA shape ([15] but see [19]). Molecular dynamics simulations have provided independent support for this view [20,21].

In support of this view, recent crystallographic analyses have suggested that the primary spine of hydration around DNA is partially occupied by monovalent cations [22]. Williams and co-workers argue that the localization of cations in the grooves of DNA should result in spontaneous DNA collapse around peaks of cation density [16]. It has further been proposed that A_{5-6} tract curvature might similarly be explained by selective cation localization in the minor groove of A_{5-6} tracts, as has been suggested from nuclear magnetic resonance (NMR) data [17].

Previous work in our laboratories tested the neutralization–collapse model through the use of a 'phantom protein' design. The binding of a cationic protein to the DNA backbone was simulated either by neutral phosphate analogs [11] or by ammonium cations tethered on flexible propyl or hexyl linkers [12,13]. Electrophoretic phasing analyses demonstrated that the modified DNA was bent in the predicted direction (i.e. towards its neutralized face). We hypothesized that the DNA bending observed in these experiments reflected collapse due to physiologically significant forces arising from asymmetries in interphosphate repulsion. Similar reasoning has subsequently been applied to DNA bending by specific proteins [23–29].

In light of the growing interest in cation density as a potential contributor to DNA curvature, we now reconsider a cluster of tethered ammonium ions as a model for studying the impact of asymmetric ion distributions on DNA shape. Our previous work demonstrated an apparent electrostatic effect between the DNA phosphate backbone and tethered hexylammonium and propylammonium cations that resulted in enhanced DNA curvature toward the neutralized region [12,13]. Acetylation to neutralize these cations eliminated induced curvature [13]. These designs supposed that ammonium ions tethered to the 5-position of pyrimidines would tend to form salt bridges with adjacent phosphate diesters, creating a patch of six neutralized phosphates, three on each side of one minor groove. Such a patch would lie on one helical face of the DNA. Since bending in the predicted direction was observed for the cationic variants, but not for neutral controls, this neutralization pattern was confirmed. It was less clear if asymmetric phosphate neutralization would result if the tethered cations occupied only the floor of the DNA major groove, rather than forming salt bridges. This issue is of interest because studies of 5-(6-aminohexyl)-2′-deoxynucleotide substitutions have suggested that tethered cations can inhibit local guanosine methylation in the major groove by *N*-methyl-*N*-nitrosourea [30,31]. This result suggests that flexible tethers allow ammonium ions to explore at least partially the major grooves, rather than exclusively form salt bridges to phosphates.

In an attempt to clarify the role of tethered ammonium ion localization in DNA bending, we have now undertaken an analysis of DNA shape when six ammonium ions are tethered on rigid propynyl chains. We predicted that such ions would have fewer degrees of freedom and their linear projection from the nucleobase would preclude their migration to the floor of the major groove. We predicted that propynyl tethers would position ammonium cations closer to DNA phosphates and enhance DNA bending due to asymmetric phosphate neutralization. However, in contrast to our chemical intuition, we report that whereas ammonium ions on flexible propyl tethers induce DNA bending in the expected direction, ammonium ions on rigid propynyl tethers do not induce DNA bending. Molecular modeling studies shed light on this result. Salt bridges

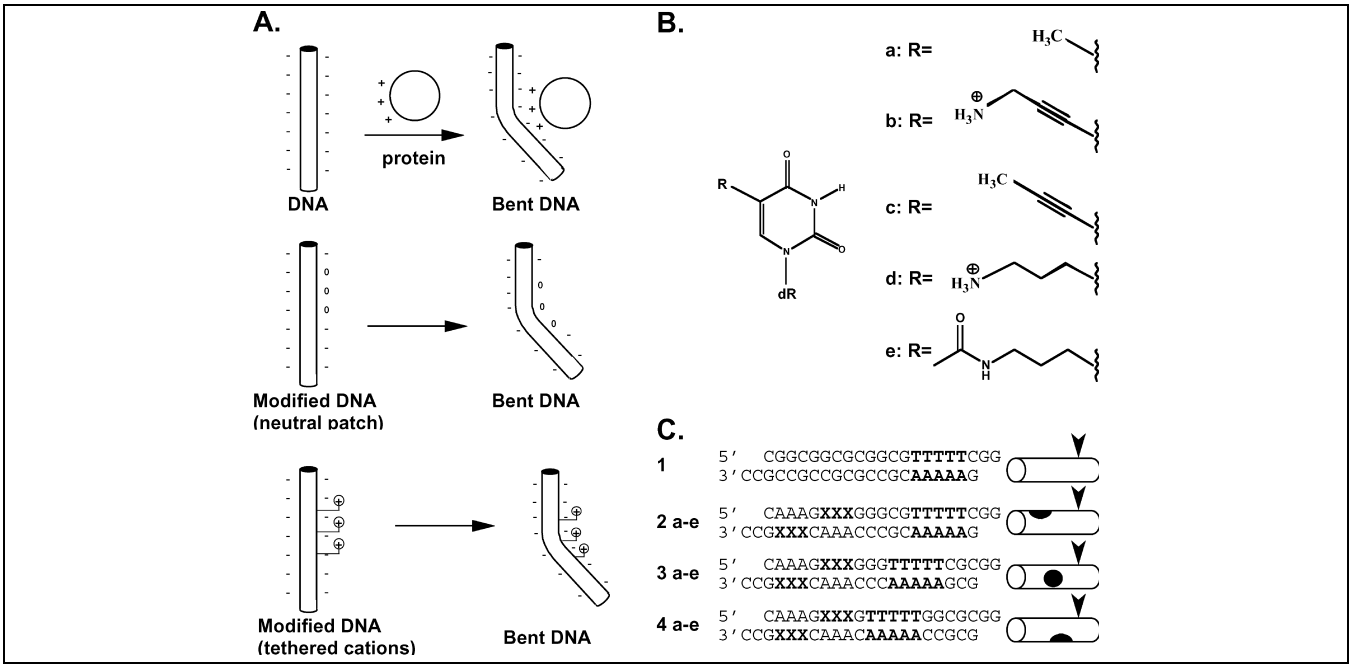

Fig. 1. Experimental model and design of DNA duplexes. A: Models of DNA bending due to electrostatic interactions. B: Structures of modified bases. dR: deoxyribose. Functions at the C5 position of deoxyuracil residues include **a**: methyl, **b**: propynylammonium, **c**: propyne, **d**: propylammonium, **e**: acetylated propylamine. C: Experimental DNA duplexes used in these studies. **1**: reference A_5 tract duplex; **2**: duplexes **2a**–**2e** in which the minor groove at the center of the modified 5′-A_3GT_3 sequence (modified residues indicated by **XXX**) is on the same helical face as the curvature due to the A_5 tract (*cis* configuration); **3**: duplexes **3a**–**3e** in which these elements are separated by ~70° (*ortho* configuration), and **4**: duplexes **4a**–**4e** in which these elements are separated by ~140° (*trans* configuration). Cylinders at the right of C depict elements of curvature found in these molecules. The concave DNA face caused by intrinsic curvature of the A_5 tract toward the minor groove is indicated by an arrowhead. Filled patches indicate the relative orientation of the 5′-A_3GX_3 test sequence with respect to the A_5 tract.

formed between ammonium ions and DNA phosphates maximize asymmetric neutralization of phosphate charges in the minor groove. Localization of ammonium ions at the center or floor of the major groove shifts the overall neutralization towards the major groove. Energetic calculations show that salt-bridged conformations are actually favored for propyl, relative to propynyl, tethers. We hypothesize that these different ammonium ion distributions dictate whether or not DNA bending will be induced, and propynyl chains actually reduce asymmetric phosphate neutralization induced by ammonium cations due to details of ion localization. Modeling suggests that propynyl tethers may further discourage salt bridge formation in situations where the double helix is curved. Finally, we note from thermal melting experiments that propyne-modified bases stabilize the double helix, raising the possibility that enhanced base stacking may make the DNA more rigid when modified by propynyl-tethered ammonium ions.

Table 1
DNA curvature data

Duplex[a]	Curvature magnitude (°)	Curvature direction (bp)[b]	T_m (°C)[c]	Helical repeat (bp/turn)	R_f (pH 6.8/8.3)[e]
a	11.9 ± 1.2	0.3 ± 0.2	44.1 ± 0.3	10.4 ± 0.1	1.00/1.00
b	13.0 ± 1.4	0.2 ± 0.1	50.7 ± 0.2	10.5 ± 0.1	0.91/0.92
c	15.1 ± 1.2[d]	0.3 ± 0.2	49.6 ± 0.1	10.4 ± 0.1	0.99/0.97
d	20.1 ± 1.6[d]	0.5 ± 0.1	39.0 ± 0.5	10.5 ± 0.1	0.94/0.93
e	10.0 ± 1.9	0.2 ± 0.1	32.1 ± 0.7	10.5 ± 0.1	1.00/0.97

[a]See Fig. 1C.
[b]Displacement of observed center of curvature (toward the minor groove) relative to the geometric center of the 5′-A_3GT_3 sequence. The indicated displacement describes how much closer to the A_5 tract is the actual reference frame of minor groove curvature at the 5′-A_3GT_3 sequence.
[c]Melting temperature of 0.5 μM DNA duplex in 10 mM sodium cacodylate, 0.2 mM EDTA, pH 7.0.
[d]Significantly different from curvature of duplex **a** (Student's *t*-test, $\alpha = 0.05$).
[e]Mobilities (relative to the corresponding unmodified form) of denatured oligonucleotides corresponding to top strands each bearing three of the covalent modifications described in Fig. 1.

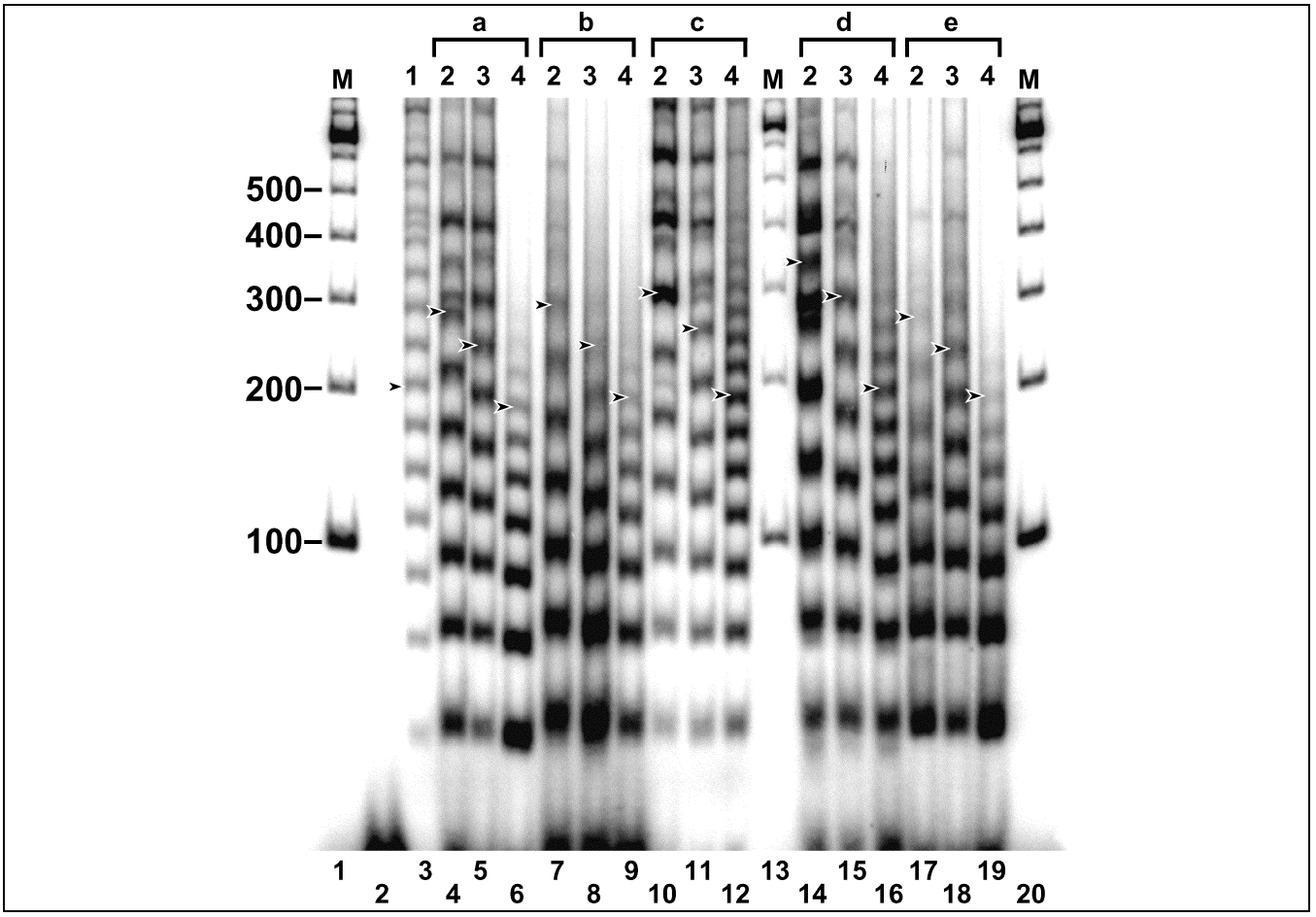

Fig. 2. Electrophoretic assay of DNA shape. DNA duplexes were ligated and analyzed by electrophoresis through 5% native polyacrylamide gels as described in Section 4. Reference lanes 1, 13, and 20 (M) contain a 100-bp duplex DNA ladder. Lane 2 contains unligated 21-bp duplex. Lanes 3–12 and 14–19 contain indicated ligated duplexes, using the designations shown in Fig. 1. Arrowheads indicate the 168-bp DNA species for each ligated sample.

2. Results and discussion

2.1. Design of DNA duplexes

Fig. 1A displays hypothetical roles of asymmetric charge neutralization in DNA deformation by cationic proteins (Fig. 1A, top), neutral phosphate analogs (Fig. 1A, middle), and tethered cations (Fig. 1A, bottom). Our previous studies suggested that DNA bending by a cationic protein can be simulated by substitution of neutral phosphate analogs [11] or by ammonium cations tethered on propyl or hexyl linkers [12,13]. In the present work we describe the synthesis and curvature analysis of DNA molecules bearing cations on either flexible or rigid three-carbon tethers. Cations were linked to the C5 position of deoxyuracil residues as shown in Fig. 1B. In addition to ammonium ions tethered on rigid propynyl linkers (Fig. 1B, structure **b**) or flexible propyl linkers (Fig. 1B, structure **d**), uncharged derivatives with methyl (Fig. 1B, structure **a**), propynyl (Fig. 1B, structure **c**), or acetylated propylamine (Fig. 1B, structure **e**) functions were synthesized and studied as controls.

Synthetic DNA duplexes (21 bp) bearing the modifications described above are shown in Fig. 1C. Duplex **1** contains a reference A_5 tract (intrinsically curved by $\sim 18°$ in a defined direction; [32]) and no other modifications. Duplexes in series **2** carry tethers **a**–**e** at the indicated positions (Fig. 1C). In this series, the locus of cur-

→

Fig. 3. Curvature analysis of DNA duplexes containing tethered cations. Graphs depict electrophoretic data for duplex **1** (triangles), duplex **2** (circles), duplex **3** (squares), and duplex **4** (crosses). Rows in the figure correspond to base modifications **a**–**e**, respectively, as indicated in Fig. 1. Apparent lengths of ligated DNA duplexes were calculated relative to mobilities of the 100-bp duplex DNA ladder. The ratio of apparent length to actual length, R_L, is a measure of DNA curvature (left column). Data were transformed and $R_L - 1$ is plotted vs. L^2 (center column). Examination of transformed data for ligated duplexes in the range 126 bp $< L <$ 189 bp allowed fitting to a phasing equation [34] for estimation of relative curvature. A plot of duplex curvature vs. radial angle (θ) was then prepared (right column) and fit by a least-squares method to a general cosine function [34], to deconvolute induced bending.

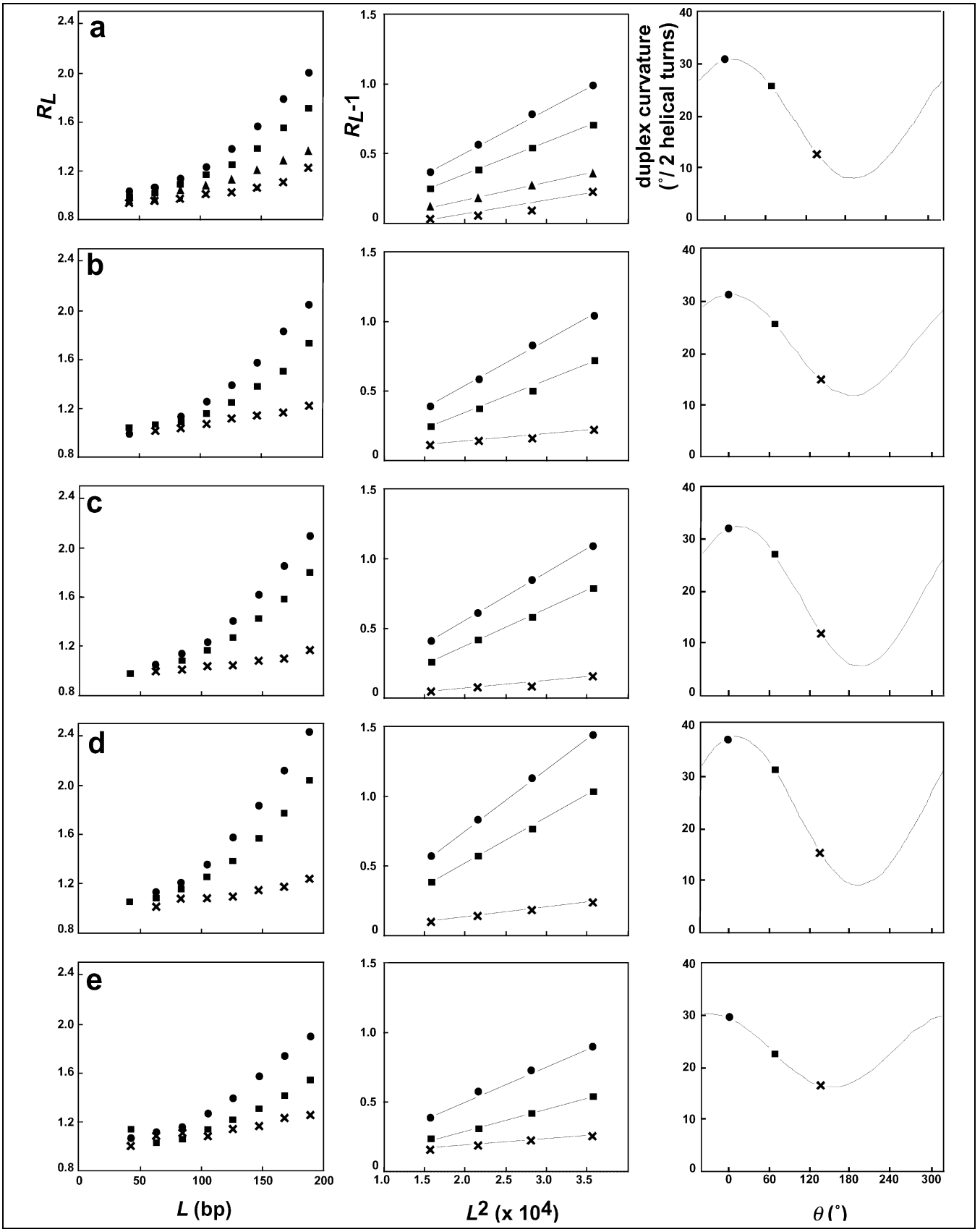
a
b
c
d
e
R_L
R_L-1
duplex curvature (°/2 helical turns)
L (bp)
L^2 (x 10^4)
θ (°)

vature of the A_5 tract is separated from the center of the 5′-A_3GT_3 sequence by 10.5 bp (*cis* configuration). The separations in duplex series **3** and series **4** are 8.5 bp (*ortho*) and 6.5 bp (*trans*), respectively.

Native gel electrophoresis provides a sensitive and semiquantitative method by which to study intrinsic DNA curvature [33]. Mobilities of DNA fragments through polyacrylamide gels exhibit both size and shape dependence. Molecules of the same molecular weight but with different shapes exhibit pronounced mobility differences. In this study, duplexes constituting two turns of the double helix were ligated into polymers to magnify intrinsic shape differences. DNA shape was then analyzed by changing the phasing of an uncharacterized site of helix deformation (the 5′-A_3GT_3 site) relative to a well-characterized reference deformation (an A_5 tract). Molecules whose deformation at 5′-A_3GT_3 sites is aligned with the reference deformation at A_5 tracts exhibit reduced electrophoretic mobility, whereas mobility is enhanced when the two deformations counteract one another.

2.2. Assays of DNA curvature

In comparing oligonucleotides bearing amines on different tethers, it was important to confirm that the amines were protonated and cationic under electrophoretic conditions. In the absence of DNA the pK_a of aminopropyne is 8.5, lower than aminopropane (pK 10–11). However, in the context of duplex DNA and local condensation of cations (including protons) amino groups on both kinds of tethers would be expected to be protonated. This was confirmed by measuring the electrophoretic mobilities of the isolated top strands of the duplexes shown in Fig. 1C under denaturing conditions. Because electrophoretic mobility is exquisitely sensitive to charge, the presence of three tethered cations is expected to retard electrophoresis. Consistent with expectations, we observed that only oligonucleotides containing propynylamine and propylamine functions were significantly retarded (Table 1). Uncharged strands bearing propynyl or acetylated propylamine functions migrated similarly to the unmodified control. These results were observed at both pH 6.8 and pH 8.3. Thus, both propynylamine and propylamine functions appear protonated in DNA under these conditions.

The helical repeat parameter (bp/helical turn) for each class of modified oligonucleotide duplexes was then determined by gel electrophoresis (data not shown; [34]). In all cases, the helical repeat was found to be 10.5 ± 0.1 bp/helical turn. Analysis of *cis*, *ortho*, and *trans* cases for each class of modified duplex was then undertaken. The results of a typical phasing experiment are shown in Fig. 2. Molecular weight markers (100-bp duplex DNA ladder) were used as mobility standards (Fig. 2, lanes 1, 13, 20). An unligated sample was electrophoresed for comparison (Fig. 2, lane 2). As modified oligonucleotide duplexes are ligated end-to-end, mobility differences among duplexes are enhanced. For ease of comparison among lanes, the 168-bp DNA species is indicated in each lane (Fig. 2, lanes 3–19). Duplex **1** served as a reference molecule lacking the 5′-A_3GT_3 sequence (Fig. 2, lane 3). The intrinsic shape of the unmodified 5′-A_3GT_3 sequence (duplexes **2a**–**4a**) was determined by changing its phasing relative to an A_5 tract (Fig. 2, lanes 4–6). These unmodified duplexes displayed different gel mobilities: the greatest retardation occurred when the minor groove of the unmodified 5′-A_3GT_3 sequence (Fig. 2, lane 4) was centered on the same DNA face as the A_5 tract (duplex **2a**, *cis* configuration). This confirms that the 5′-A_3GT_3 sequence is intrinsically curved toward the minor groove as was previously suggested [13].

The effect of propylammonium groups on DNA mobility was studied by electrophoresis of duplexes **2d**–**4d** (Fig. 2, lanes 14–16). The increased difference between *cis* and *trans* configurations immediately confirmed our previous observation that the distribution of cations on flexible propyl tethers induces additional bending toward the minor groove. When thymines in the 5′-A_3GT_3 sequence carried neutral acetylated propylammonium tethers **2e**–**4e** (Fig. 2, lanes 17–19), gel mobility anomalies were comparable to those observed for unmodified duplexes **2a**–**4a** (Fig. 2, lanes 4–6). These observations confirm our previous report [13], but employ a more appropriate reference molecule (duplex **1**).

A different effect is observed for duplexes containing rigid propynylammonium groups (**2b**–**4b**). In this case, no qualitative difference in mobility anomaly relative to **2a**–**4a** was observed (Fig. 2, compare lanes 7–9 with lanes 14–16). Thus, DNA bending is not induced in the 5′-A_3GT_3 sequence by six propynylammonium cations. Neutral duplexes (**2c**–**4c**), in which the ammonium cation is removed from the propynyl group, displayed a very modest increase in the intrinsic curvature at the 5′-A_3GT_3 sequence (Fig. 2, lanes 10–12).

Quantitative estimates of both the magnitude and direction of intrinsic and induced curvature were deduced from plots of the electrophoretic data (Fig. 3) as described [34]. DNA shape information is first depicted graphically by plotting R_L (the ratio of apparent DNA length to actual DNA length) vs. actual DNA length. These results are shown in the left column of Fig. 3. The data were then transformed to allow fitting to a linear function relating gel anomaly to the relative curvature for each phasing (Fig. 3, center column). Curvature parameters were then extracted from the resulting linear functions and used to construct a phasing relationship (Fig. 3, right column) to estimate both the magnitude and direction of bending.

As shown in Table 1, the unmodified 5′-A_3GT_3 test sequence is intrinsically curved by $\sim 12°$ toward the minor groove at the center of the sequence, as previously reported [13]. Propylammonium groups (**d**) increased the curvature at the test sequence by $\sim 8°$, while acetylated

propylammonium groups (**e**) had no effect on curvature, confirming our previous result [13]. In contrast, tethering of ammonium cations on rigid propynyl chains (**b**) did not significantly increase DNA curvature. Surprisingly, neutral propynyl groups alone (**c**) caused a modest but statistically significant increase ($\sim 3°$) in curvature toward the minor groove. Table 1 also indicates that in all cases, the reference frame for compression of the minor groove at the 5′-A_3GT_3 sequence lies within 0.5 bp from the geometric center of the sequence, as expected.

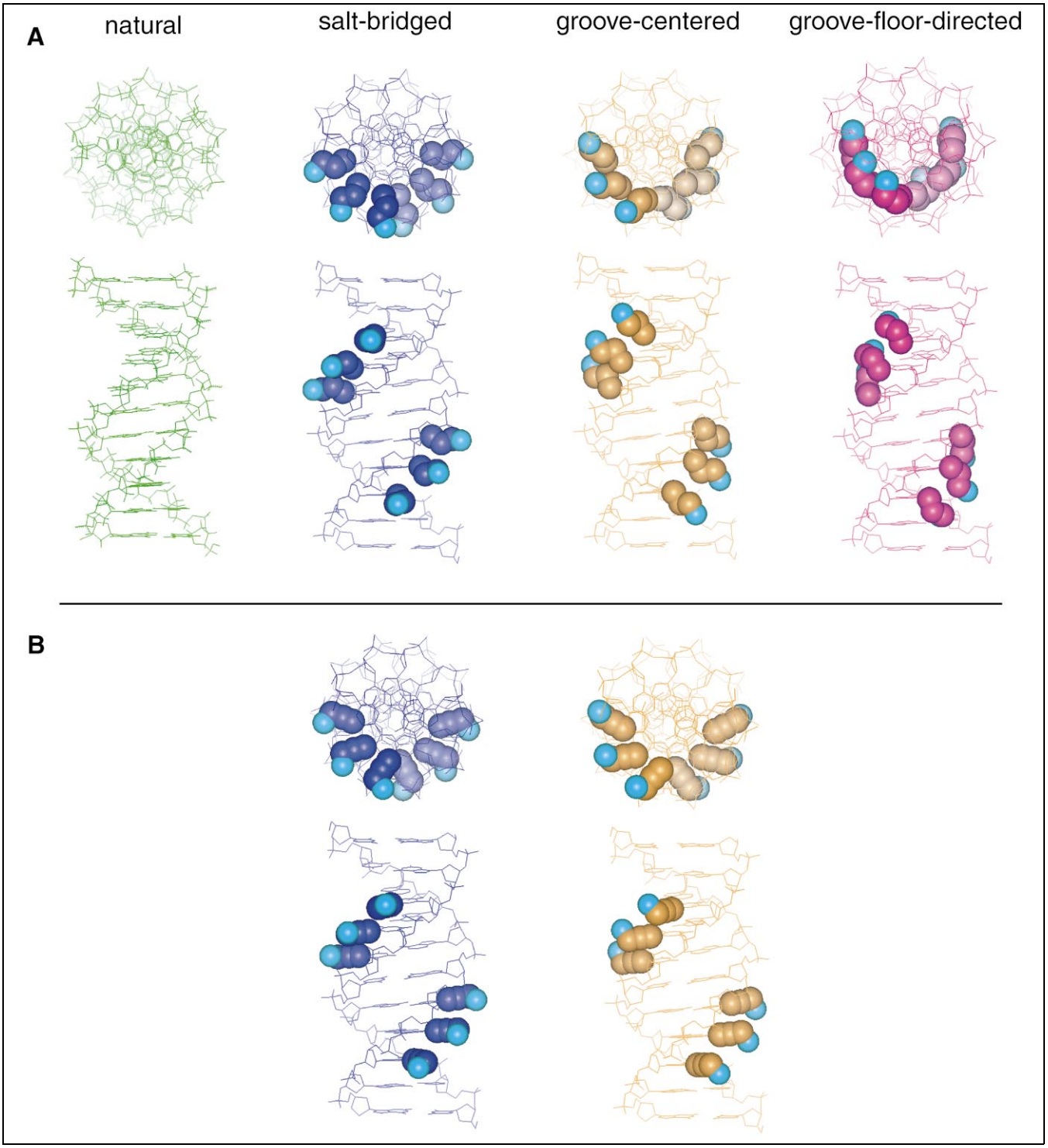

Fig. 4. Limiting models of ammonium ion positions in DNA duplexes with the core of the sequence used for bending studies: CCAAAGX′X′X′GG. A: Limiting models for propyl-tethered ammonium ions where X′ = 5-ω-aminopropyluracil; dark blue = salt-bridged, orange = groove-centered, magenta = groove-floor-directed, and light blue = nitrogen atom. B: Limiting models for propynyl-tethered ammonium ions where X′ = 5-ω-aminopropynyluracil.

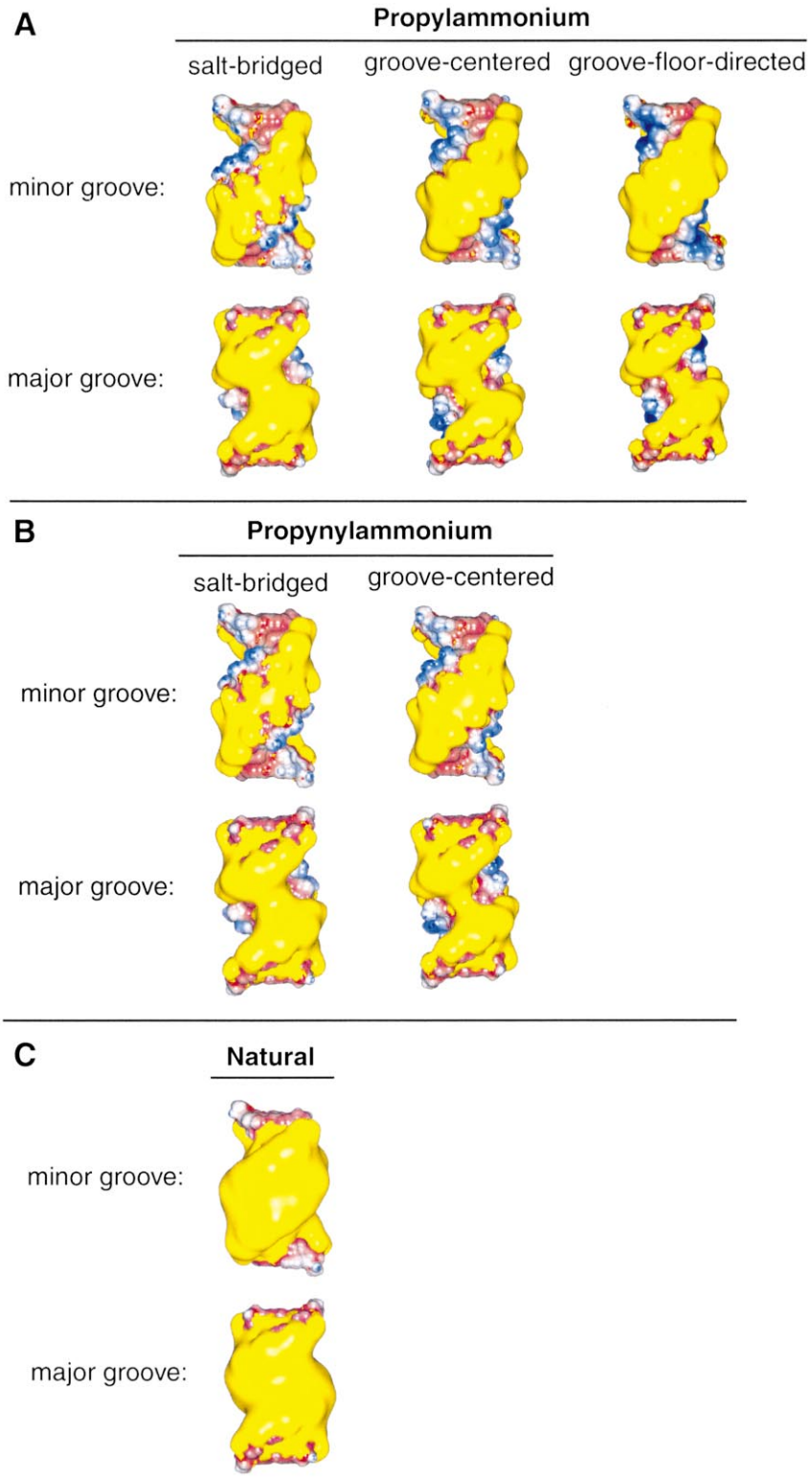

Fig. 5. Graphical display of negative electrostatic potential contours (−3 *kT*/mol/e) for the tethered ion conformations from Fig. 4 (identical helix orientations are shown in Fig. 4 and this figure). DNA duplexes are represented as solvent accessible surfaces onto which are mapped surface electrostatic potentials. Calculations were performed using Delphi implemented through Insight. Parameters included solute $\varepsilon = 4.0$, solvent $\varepsilon = 80$, and ionic strength = 0.145 mM. Yellow contours give −3 *kT*/mol/e negative electrostatic potentials. Solvent accessible surface negative potential is shaded red and positive potential is shaded blue. A: Negative electrostatic potentials for limiting models of propylammonium ions. B: Negative electrostatic potentials for limiting models of propynylammonium ions. C: Negative electrostatic potentials for the same DNA sequence when unmodified.

2.2. Assays of DNA thermal stability

We considered the possibility that enhanced base stacking between propynyl-modified pyrimidines might overcome unbalanced electrostatic forces and mask charge collapse [30,31,35–38]. We therefore analyzed the thermal stabilities of duplexes **2a**–**2e**. Table 1 shows that propynylammonium (**b**) and propynyl (**c**) modifications at the 5′-A_3GT_3 sequence resulted in significant (∼6°C) duplex stabilization relative to the unmodified sequence (**a**). Propylammonium (**d**) and acetylated propylammonium (**e**) modifications had the opposite effect, destabilizing the duplex by ∼5° and ∼12°, respectively (Table 1). Stabilization of the double helix by propynyl-tethered cations and destabilization by propyl-tethered cations suggests that cation tethering is not strongly stabilizing per se. Rather, the nature of the tether seems to either stabilize (propynyl) or destabilize (propyl) DNA stacking. The potential for enhancement of stacking interactions by propynyl-modified pyrimidines has been suggested [39]. The basis for helix destabilization by propyl tethers is unclear. In addition to determination of melting temperatures, we estimated both enthalpy and entropy parameters for duplexes **2a**–**2e** by analysis of melting curves (data not shown). The estimated enthalpy and entropy parameters predicted duplex melting temperatures that agreed precisely with the measured values. Estimated thermodynamic parameters suggested that melting of duplexes **2a** (unmodified) and **2c** (propynyl) was accompanied by compensating enthalpy and entropy values that were approximately two-fold higher than those for the three other duplexes. However, no obvious trends were observed that further illuminate why certain tethered cations result in bending of DNA (propylammonium), while others do not (propynylammonium).

2.3. Simulation of tethered cation localization and charge neutralization

We wished to use molecular modeling to explore (i) the extent to which ammonium ion localization affects charge asymmetry in DNA and (ii) the relative energetics of different ammonium ion localization. Two modeling approaches were therefore undertaken to assess the effects of propyl- and propynyl-tethered cations on DNA. The first approach involved the creation of limiting models

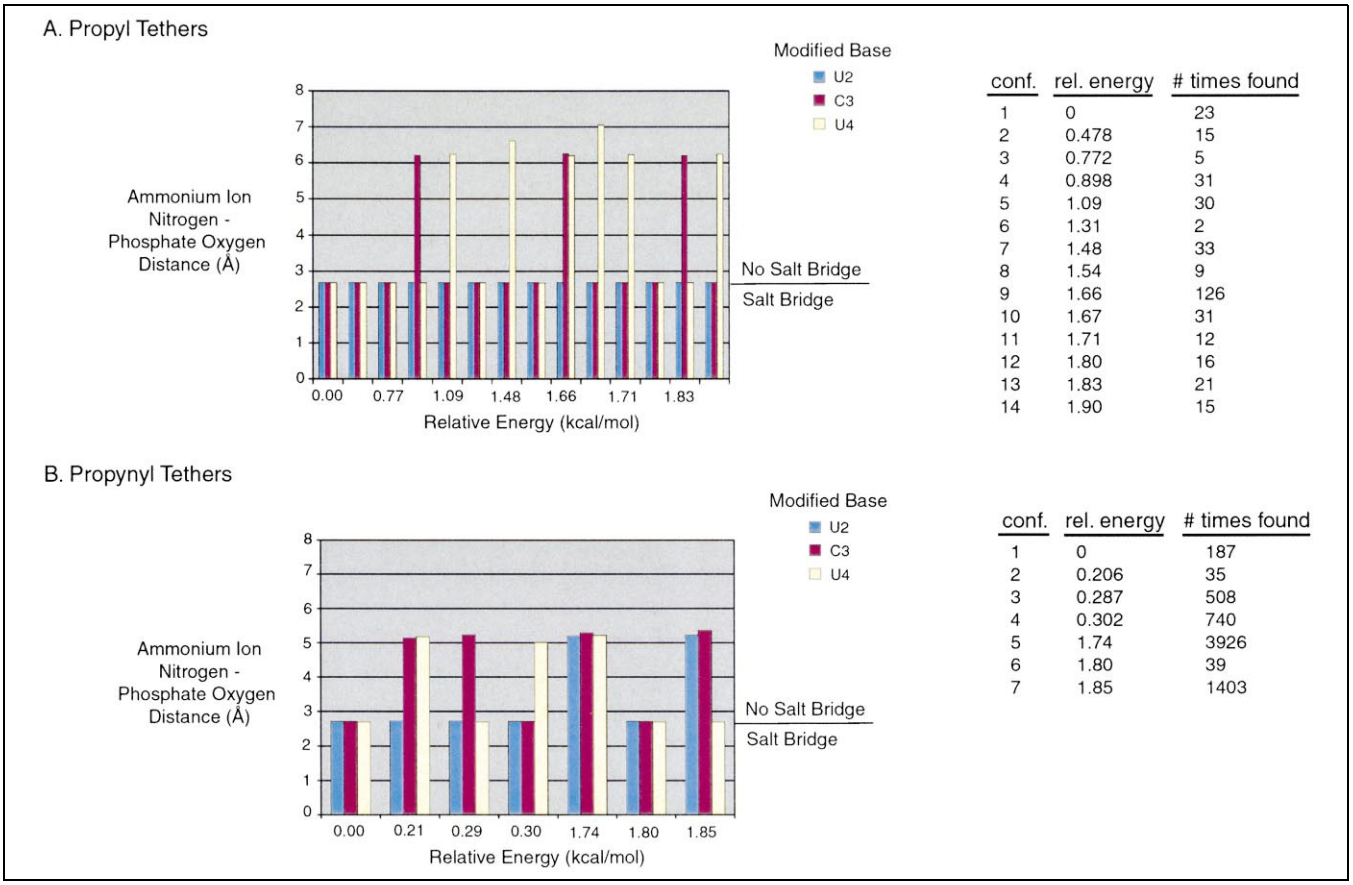

Fig. 6. Non-bridging phosphate oxygen-tethered ammonium nitrogen atom distances versus conformational energy for DNA duplexes of sequence: $A_1U_2'C_3'U_4'T_5$ where subscripts refer to the sequential order of the nucleotides and the prime superscript refers to a nucleobase appended at the 5-position with either an ω-propylammonium group (A) or an ω-propynylammonium group (B). 'Conf.' refers to conformation numbered consecutively from lowest to highest energy. '# times found' refers to the number of times a given conformation was found during the Monte Carlo conformational search, and may be used to infer completeness.

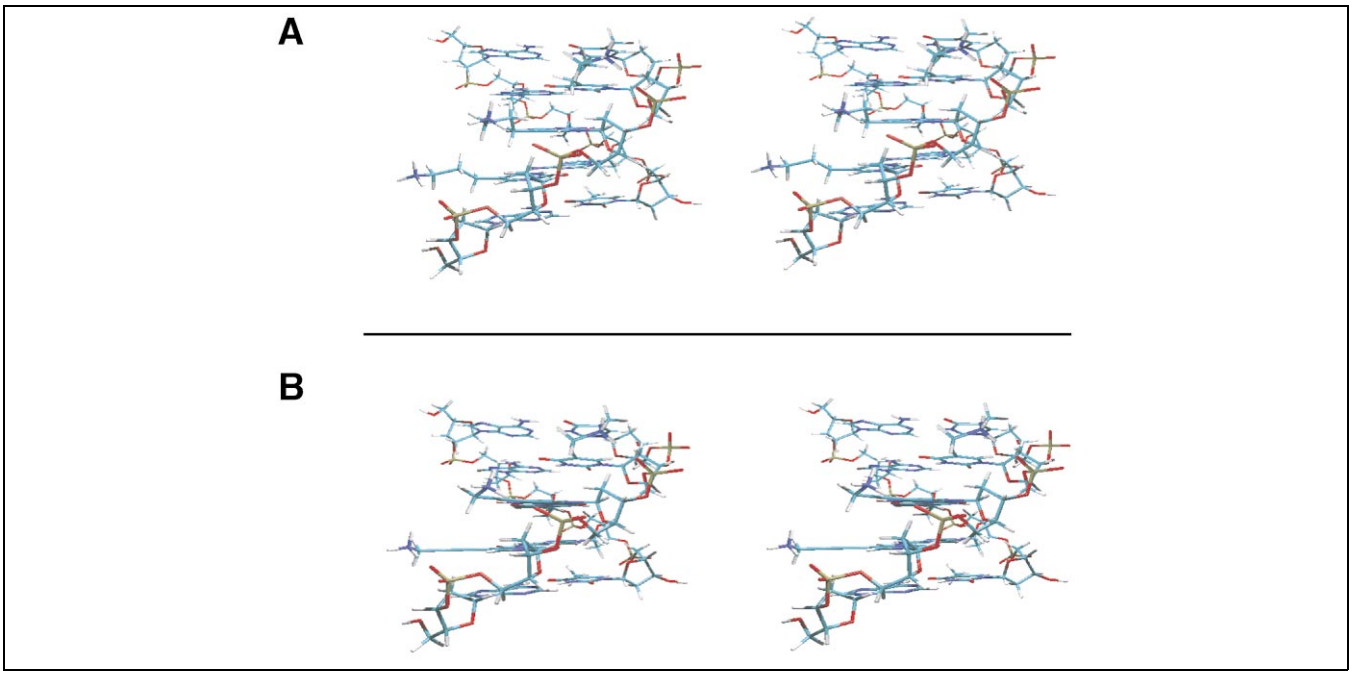

Fig. 7. Representative conformations of propylammonium and propynylammonium duplexes found during MCMM conformational searches. A: Stereo view of conformer 1 (0 kcal/mol relative energy) from Fig. 6A (propylammonium). B: Stereo view of conformer 1 (0 kcal/mol relative energy) from Fig. 6B (propynylammonium).

for side chain orientation by initial manual manipulation of side chain torsion angles, followed by molecular mechanics minimization of three local minima for the tethered ions: salt-bridged, groove-centered and groove-floor-directed (Fig. 4). Negative electrostatic potentials were then calculated for each of the limiting tethered ion conformations, the results of which are displayed graphically in Fig. 5. Consistent with fewer degrees of freedom associated with the propynyl tether, only salt-bridged and groove-centered conformations are depicted in panel B of Figs. 4 and 5. Fig. 5 suggests asymmetric charge neutralization with salt-bridged propyl- and propynyl-tethered ammonium ions based on negative electrostatic potentials in the minor and major grooves (minimal negative electrostatic potential is observed in the minor groove of modified duplexes; left column). In contrast, negative electrostatic potentials for groove-centered and groove-floor-directed tethered ammonium ions in Fig. 5 suggest more laterally symmetric charge neutralization (Fig. 5A, center and right). It follows from this analysis that the magnitude and direction of DNA bending will depend on the relative contributions of the three limiting conformers: DNA bending towards the minor groove is enhanced to the extent that salt-bridged ammonium ion distributions are favored. Based on the absence of DNA bending for the propynyl-tethered ammonium ions, we hypothesize that salt-bridged conformations are more favorable for propyl-tethered ammonium ions, where tether flexibility is greater.

To test this notion, the second modeling approach then used Monte Carlo multiple minimum (MCMM) conformational searching to predict the preferred conformations of tethered ammonium ions [40]. Simulations were conducted on standard B-DNA duplex coordinates of sequence 5′-ATCTT. The central three pyrimidine residues were appended at their 5-positions with either ω-ammonium propyl or ω-ammonium propynyl groups to evaluate the conformational behavior of the two tethered cation types, yielding 5′-$A_1U_2'C_3'U_4'T_5$ (where subscripts refer to the sequential order of the nucleotides). The results of MCMM conformational searches in each tether series are summarized in Fig. 6 for the conformers found within a 0–2 kcal/mol window. During the simulations, duplex coordinates were frozen except for the ammonium ions and tethers. Shown for the two series of tether types are heavy atom distances between the ammonium ion nitrogen atom and the nearest non-bridging 5′-phosphate oxygen for each residue for each unique conformer found, along with relative conformer energies. An N–O distance of ~2.7 Å was found consistently when a salt bridge formed between the ammonium and phosphate ions. Results for the propylammonium-modified duplex, summarized in Fig. 6A, indicate salt bridge formation for all three modified residues, but in decreasing extent as a function of energy, through the series U_2' (14 of 14 conformers), C_3' (11 of 14 conformers), and U_4' (eight of 14 conformers). Overall, salt-bridged conformations were found in 33/42 cases (79%). In the case of the propynylammonium series (Fig. 6B), all three modified residues formed some salt bridges, and non-salt-bridged conformations were ap-

proximately evenly distributed across the three residues. Interestingly, non-salt-bridged conformers are more common for propynyl tethers, than for propyl tethers, occurring in 9/21 cases (43%). Stereo representations of the lowest energy conformations found by MCMM searching are given in Fig. 7. These results support the notion that propylammonium groups bend DNA, whereas propynylammonium groups do not bend DNA, because the former prefer salt-bridged conformations that maximize charge asymmetry.

The above modeling results do not take into account DNA flexibility or bending. The latter was examined briefly using model DNA coordinates for nucleosomes created by Sussman and Trifonov (data not shown; [41]). Both propynylammonium and propylammonium tethers gave conformers less biased toward salt bridges, but the bias away from salt bridge formation was more acute for the propyne series. Irrespective of how well the DNA coordinates model bending in the present results, this finding suggests propynyl tethers, due to their inherent rigidity, may be generally at a disadvantage in comparison to propyl tethers in responding to deformations of the double helix that attend bending. Indeed, propynyl tethers, as a result of their rigidity, couple the motions of ammonium ions to the plane of a base pair, and thereby remove the possibility for independent movement of these two entities (with the exception of limited rotation possible from moving the ammonium ion in an arc about an axis passing through the alkynyl carbons).

2.4. Interplay of molecular forces and phosphate repulsion

We considered four concepts to explain the absence of DNA bending induced by tethering propynylammonium cations, in contrast to propylammonium cations. First, although there is experimental evidence that cations on flexible propyl tethers may sample the DNA major groove [31], our modeling results suggest that such conformations shift the asymmetry of residual electric charge towards the major groove (Fig. 5). In contrast, salt-bridged conformations of both propylammonium and propynylammonium groups maximize asymmetric charge neutralization of the minor groove (Fig. 5). This result suggests that the absence of DNA bending by propynylammonium ions might be explained if propynylammonium ions are less prone to salt bridging than propylammonium ions. Second, our energy calculations (Fig. 6) confirm this hypothesis. In contrast to our initial intuition, rigid propynylammonium groups actually are more prone to sample groove-centered conformations than are propylammonium groups (Fig. 6, compare A and B). Third, we observed a marked thermal stabilization of the double helix only in the case of the propynylammonium substitutions. We therefore suggest the possibility that enhanced thermal stability accompanies favorable interactions between modified bases and might enhance DNA stiffness. Fourth, we suggest the possibility that conformational biases disfavor the bent state because it leads to diminished salt bridging in bent DNA with rigid propynyl groups.

3. Significance

Our work illuminates the notion that specific cation distributions in the DNA grooves may influence DNA shape. We suggest that different cation locations create charge neutralization patterns with very different degrees of asymmetry. In the present case, cations that migrate into the grooves erode the lateral asymmetry present when they form salt bridges with phosphates. A related argument has been proposed to explain how the localization of mobile free ammonium ions might cause differential curvature of 5′-A_4T_4 vs. 5′-T_4A_4 tracts [17]. We further suggest that enhanced base–base interactions or restricted cation mobility can also mitigate against induced bending due to unbalanced phosphate repulsion.

4. Materials and methods

4.1. Oligonucleotides

Unmodified oligonucleotides were prepared using an ABI model 394 DNA synthesizer according to standard procedures and were deprotected in hot ammonia. Oligomers were purified by electrophoresis through 20% polyacrylamide gels containing 7 M urea, eluted, desalted using C_{18} reverse phase cartridges, and characterized by microspray mass spectrometry (MS). Oligonucleotides containing propylamines were synthesized and deprotected as previously described [42,43]. Oligonucleotides containing propynylamines were synthesized and deprotected as described below. Mass spectrophotometric analysis revealed that oligonucleotides containing propynylamines were prone to nucleophilic attack on carbonyl compounds. Attempted purification in urea gels after thermal denaturation in either 7 M urea or neat formamide resulted in significant levels of propynylamine acylation by the denaturant. In contrast, the purity of propynylamine oligonucleotides purified by electrophoresis without heating in the presence of denaturant was confirmed by MS. Mass spectra were also taken after phosphorylation and annealing of duplexes to ensure that propynylamines were not modified during radiolabeling.

4.2. 5-(3-N-(Trifluoroacetyl)aminopropynyl)-5′-O-(4,4′-dimethyltrityl)-2′-deoxyuridine

To a mixture of 5-(3-*N*-(trifluoroacetyl)aminopropynyl)-2′-deoxyuridine [42] (173 mg, 0.458 mmol) and 4,4′-dimethoxytrityl chloride (186 mg, 0.55 mmol) was added pyridine (2 ml). After stirring for 4 h at room temperature, 10 ml of CH_2Cl_2 was added, and the mixture was extracted with 5% aqueous $NaHCO_3$, dried over Na_2SO_4, and concentrated. Flash chromatography (SiO_2, pyridine (1%)/MeOH (3%)/CH_2Cl_2) provided 5-(3-*N*-(trifluoroacetyl)aminopropynyl)-5′-*O*-(4,4′-dimethyltrityl)-2′-deoxyuri-

dine: 248 mg, 80% yield: ^{1}H NMR ($CDCl_3$) δ 2.17–2.57 (m, 2 H), 2.35 (s, 2 H), 3.32–3.46 (m, 2 H), 3.79 (s, 6 H), 3.92 (t, 2 H, J = 5.7 Hz), 4.11 (d, 2 H, J = 3.3 Hz), 4.59 (br, 1 H), 6.34 (t, 1 H, J = 6.9 Hz), 6.55 (br, 1 H), 6.85 (d, 4 H, J = 8.7 Hz), 7.13–7.43 (m, 9 H), 8.25 (s, 1 H), 8.60 (br, 1 H); MS (FAB^+) *m/z* 679 (M^+); HRMS (FAB^+) calculated for $C_{35}H_{32}F_3N_3O_8$ 679.2142 (M^+), found 679.2155.

4.3. 5-(3-N-(Trifluoroacetyl)aminopropynyl)-5′-O-(4,4′-dimethyltrityl)-2′-deoxyuridine 2-cyanoethyl N,N-diisopropyl phosphoramidite

To a solution of 5-(3-*N*-(trifluoroacetyl)aminopropynyl)-5′-*O*-(4,4′-dimethyltrityl)-2′-deoxyuridine (238 mg, 0.35 mmol) in CH_2Cl_2 (2.0 ml) was added diisopropylamine (0.148 µl, 1.05 mmol) and 2-cyanoethyl *N*,*N*-diisopropylchlorophosphine (0.102 µl, 0.46 mmol) successively at room temperature. The mixture was stirred for 2 h, followed by dilution with 30 ml of CH_2Cl_2, extraction with 5% aqueous $NaHCO_3$, drying over Na_2SO_4, and concentration. Purification by flash chromatography (SiO_2, MeOH (3%)/Et_3N (1%)/CH_2Cl_2) gave the phosphoramidite, 287 mg (91%), as a mixture of two diastereomers, with a small amount of $HPO(OCH_2CH_2CN)N(iPr)_2$ as an inseparable impurity (^{31}P NMR δ 13.84), 91:9: ^{1}H NMR selected signals of diastereomers δ 2.44 (t, 2 H, J = 6.3 Hz, -OCH_2CH_2CN), 2.62 (t, 2 H, J = 6.3 Hz, –OCH_2CH_2CN), 3.78 (s, 3 H, OMe), 3.79 (s, 3 H, OMe), 4.17 (m, 1 H, H_4'), 4.22 (m, 1 H, H_4'), 4.6–4.8 (m, 2 H, H_3'), 6.29 (m, 1 H, H_1'), 6.31 (m, 1 H, H_1'), 8.23 (s, 1 H), 8.27 (s, 1 H); ^{31}P NMR ($CDCl_3$) δ 148.36, 148.62; MS (FAB^+) *m/z* 902 (MNa^+); HRMS (FAB^+) calculated for $C_{44}H_{49}F_3N_5O_9P$ 902.3117 (MNa^+), found 902.3146.

4.4. Synthesis of aminopropargyl oligonucleotides

All oligonucleotides were synthesized trityl-off using a controlled pore glass support via the phosphite-triester method with an Applied Biosystems 391EP DNA synthesizer (1 µmol scale). Removal of the cyanoethyl groups was accomplished by treating the solid support with 0.05 M DBU in pyridine for 4 h at room temperature, followed by removal of the oligonucleotide from the solid support and base deprotection using concentrated NH_4OH for 2 h at 55°C.

4.5. Micro-electrospray ionization (µESI)-MS

Samples were desalted by sequential gel filtration (Chroma Spin Columns, Clontech Laboratories, Inc., Palo Alto, CA, USA) and passage through a cation exchange cartridge (Optiguard, SIS Inc., Ringoes, NJ, USA). Samples were then directly infused into a MAT 900 mass spectrometer (Finnigan Corporation, Bremen, Germany) of electrostatic analyzer magnet (EB) geometry using µESI in negative mode. Flow rates of 0.3 µl/min were used in conjunction with SF_6 gas to prevent source corona discharge. The µESI source voltage was set to ~3.6 kV and the capillary temperature to ~180°C. The magnet was scanned from *m/z* 600 to 3000 at a rate of 10 s/decade. The position- and time-resolved ion counter was used for ion detection. Several scans were collected and summed, and the multiply charged spectra were transformed by the Finnigan MAT software to give M_r values.

4.6. Ligation ladders

Purified oligonucleotides (400 pmol) were radiolabeled using polynucleotide kinase and [γ-^{32}P]ATP (10 µCi; 3000 Ci/mmol) in 10 µl reactions containing 8 U T4 polynucleotide kinase in the buffer recommended by the manufacturer (New England Biolabs). Incubation was for 45 min at 37°C, followed by addition of unlabeled ATP to 4 mM and further incubation for 20 min. Equal amounts (169 pmol) of labeled complementary oligomers were then mixed in a volume of 10 µl, heated to 80°C and cooled gradually to 4°C. The annealed oligonucleotides were then assembled into ligation reactions (10 µl) containing 400 U T4 DNA ligase in the buffer recommended by the manufacturer (New England Biolabs). A small fraction of unligated duplex was retained as a marker for gel studies. Ligation reactions were incubated at 22°C for 30 min, and terminated by addition of EDTA to a final concentration of 30 mM.

4.7. Exonuclease treatment

In cases where it was necessary to distinguish circular vs. linear ligation products, *Bal*31 exonuclease was used to degrade linear products, while sparing DNA circles. Exonuclease treatment was performed by adding 5 µl 2× *Bal*31 exonuclease reaction buffer and 1 U *Bal*31 exonuclease (New England Biolabs) to 4 µl of ligation product, followed by incubation at 30°C for 30 min prior to electrophoresis.

4.8. Electrophoretic analysis

Ligation ladders were analyzed on 5% native polyacrylamide gels (1:29 bisacrylamide:acrylamide) prepared in 1× TBE buffer. Electrophoresis was at 10 V/cm at 22°C. Molecular weight markers were created by labeling a 100-bp DNA ladder (Gibco) using T4 DNA polymerase (New England Biolabs) and [α-^{32}P]dATP as recommended by the ladder manufacturer. Gels were dried and exposed to storage phosphor screens for analysis using a Molecular Dynamics Storm 840 phosphorimager.

4.9. DNA curvature analysis

Curve fitting was performed using Kaleidagraph™ software running on a power Macintosh computer. Estimation of the helical repeat parameter (bp/helical turn) for experimental DNA samples, as well as the magnitude (t) and direction (D) of DNA curvature with respect to the internal A_5 tract reference was performed as described [34]. In this procedure, the DNA helical repeat is determined by extrapolation as the base pair spacing between A_5 tracts that maximizes the electrophoretic anomaly due to curvature at these tracts. DNA curvature induced by tethered cations is estimated by deconvolution of relative curvature plots measured for oligomers with patches of six modifications flanking the DNA minor groove in *cis*, *ortho*, or *trans* positions, relative to the internal A_5 tract reference curvature element [34]. The curvature (helix axis deflection) at the test sequence is given in degrees by parameter t. The direction of curvature is given as D, which describes the discrepancy (in bp) between the actual center of bending of the test sequence, and the geometric center of the sequence assigned for calculation [34].

4.10. T_m determination

Solutions of DNA duplexes contained 0.5 μM complementary oligonucleotides in 10 mM sodium cacodylate, 0.2 mM EDTA, pH 7.0. Melting experiments were performed in 1 cm path length quartz cuvettes using a Varian Cary 300Bio UV-visible spectrophotometer equipped with a thermoprogrammer. Samples were heated to 95°C for 1 min and then cooled to 5°C over 30 min. UV absorbance at 260 nm was then monitored as the sample temperature was increased from 5°C to 95°C at a rate of 0.5° per min. Nitrogen was flushed continuously through the sample chamber to prevent condensation. The melting sample temperature (T_m) was derived by computer fitting of the denaturation data, using a previously described two-state model for melting [44].

4.11. Molecular modeling

Conformational searching on DNA duplexes was performed via the MCMM method [40] implemented by Macromodel, version 6.5 (Schrodinger, Inc.). The amber* forcefield, based on the Kollman all atom forcefield, provided within the program was used [45]. Phosphate non-bridging oxygen partial charges of −0.85 were used. All calculations were performed with core duplex atoms frozen, and the GB/SA solvent model for water [46]. The ability of the amber* forcefield (under gas phase conditions) to reproduce the relative energies of deformed uracil bases bearing ammonium propynyl substituents obtained by ab initio Hartree-Fock calculations (HF/6-31G*/HF/6-31G*) in the gas phase was investigated briefly by excising ammonium propynyl U2 and ammonium propynyl U4 bases from one of the higher energy structures obtained from the MCMM simulation (see Fig. 5 for nomenclature). In these cases the forcefield calculation was found to recover 80–90% of the ab initio calculated energy. Negative electrostatic potentials were calculated using Delphi as implemented in Insight 98 (Molecular Simulations Inc.).

Acknowledgements

We thank M. Doerge in the Mayo Foundation Molecular Biology Core Facility for providing excellent oligonucleotide synthesis services, L. Benson in the Mayo Biomedical Mass Spectrometry Core Facility for analytical assistance, and M. Gacy and P. Hoyne for assistance with thermal melting experiments. R.B.D. was a recipient of a Summer Undergraduate Research Fellowship from Mayo Graduate School. Supported by the Mayo Foundation and NIH Grant GM54411 (L.J.M.), and the National Aeronautics and Space Administration (C.S.).

References

[1] J.D. Kahn, D.M. Crothers, DNA bending in transcription initiation, in: Cold Spring Harbor Symposia on Quantitative Biology, Vol. LVIII, Cold Spring Harbor Laboratory Press, Cold Spring Harbor, NY, 1993, pp. 115–122.
[2] K. Zahn, F.R. Blattner, Direct evidence for DNA bending at the lambda replication origin, Science 236 (1987) 416–422.
[3] R. Schlief, Why should DNA loop?, Nature 327 (1987) 369–370.
[4] S.C. Schultz, G.C. Shields, T.A. Steitz, Crystal structure of a CAP–DNA complex: The DNA is bent by 90°, Science 253 (1991) 1001–1007.
[5] K. Luger, A.W. Mader, R.K. Richmond, D.F. Sargent, T.J. Richmond, Crystal structure of the nucleosome core particle at 2.8 Å resolution, Nature 389 (1997) 251–260.
[6] L.J. Maher, Mechanisms of DNA bending, Curr. Opin. Chem. Biol. 2 (1998) 688–694.
[7] Y. Kim, J.H. Greiger, S. Hahn, P.B. Sigler, Crystal structure of a yeast TBP/TATA-box complex, Nature 365 (1993) 512–520.
[8] A. Pontiggia, R. Rimini, V.R. Harley, P.N. Goodfellow, R. Lovell-Badge, M.E. Bianchi, Sex-reversing mutations affect the architecture of SRY–DNA complexes, EMBO J. 13 (1994) 6115–6124.
[9] G.S. Manning, The molecular theory of polyelectrolyte solutions with applications to the electrostatic properties of polynucleotides, Q. Rev. Biophys. 11 (1978) 179–246.
[10] G.S. Manning, K.K. Ebralidse, A.D. Mirzabekov, A. Rich, An estimate of the extent of folding of nucleosomal DNA by laterally asymmetric neutralization of phosphate groups, J. Biomol. Struct. Dyn. 6 (1989) 877–889.
[11] J.K. Strauss, L.J. Maher, DNA bending by asymmetric phosphate neutralization, Science 266 (1994) 1829–1834.
[12] J.K. Strauss, C. Roberts, M.G. Nelson, C. Switzer, L.J. Maher, DNA bending by hexamethylene-tethered ammonium ions, Proc. Natl. Acad. Sci. USA 93 (1996) 9515–9520.
[13] J.K. Strauss, T.P. Prakash, C. Roberts, C. Switzer, L.J. Maher, DNA bending by a phantom protein, Chem. Biol. 3 (1996) 671–678.
[14] L.D. Williams, L.J. Maher, Electrostatic mechanisms of DNA deformation, Annu. Rev. Biophys. Biomol. Struct. 29 (2000) 497–521.
[15] L. McFail-Isom, C.C. Sines, L.D. Williams, DNA structure: cations in charge?, Curr. Opin. Struct. Biol. 9 (1999) 298–304.
[16] X.Q. Shui, C.C. Sines, L. McFail-Isom, D. VanDerveer, L.D. Williams, Structure of the potassium form of CGCGAATTCGCG: DNA deformation by electrostatic collapse around inorganic cations, Biochemistry 37 (48) (1998) 16877–16887.
[17] N.V. Hud, J. Feigon, Localization of divalent metal ions in the minor groove of DNA A-tracts, J. Am. Chem. Soc. 119 (1997) 5756–5757.
[18] N.V. Hud, V. Sklenar, J. Feigon, Localization of ammonium ions in the minor groove of DNA duplexes in solution and the origin of DNA A-tract bending, J. Mol. Biol. 286 (1999) 651–660.
[19] T.K. Chui, M. Kaczor-Grzeskowiak, R.E. Dickerson, Absence of minor groove monovalent cations in the crosslinked dodecamer C-G-C-G-A-A-T-T-C-G-C-G, J. Mol. Biol. 292 (1999) 589–608.
[20] D. Hamelberg, L. McFail-Isom, L.D. Williams, W.D. Wilson, Flexible structure of DNA: ion dependence of minor-groove structure and dynamics, J. Am. Chem. Soc. 122 (2000) 10513–10520.
[21] M.A. Young, B. Jayaram, D.L. Beveridge, Intrusion of counterions into the spine of hydration in the minor groove of B-DNA: fractional occupancy of electronegative pockets, J. Am. Chem. Soc. 119 (1997) 59–69.
[22] X. Shui, L. McFail-Isom, G.G. Hu, L.D. William, The B-DNA dodecamer at high resolution reveals a spine of water on sodium, Biochemistry 37 (1998) 8341–8355.
[23] R. Gurlie, K. Zakrzewska, DNA curvature and phosphate neutralization: an important aspect of specific protein binding, J. Biomol. Struct. Dyn. 16 (1998) 605–618.
[24] R. Gurlie, T. Duong, K. Zakrzewska, The role of DNA–protein salt bridges in molecular recognition: a model study, Biopolymers 49 (1999) 313–327.
[25] T.K. Kerppola, T. Curran, The transcription activation domains of Fos and Jun induce DNA bending through electrostatic interactions, EMBO J. 16 (1997) 2907–2916.
[26] S. Sanghani, K. Zakrzewska, R. Lavery, Modeling DNA bending induced by phosphate neutralization, in: R. Sarma, M. Sarmi (Eds.), Biological Structure and Dynamics, Vol. 2, Adenine Press, Schenectady, NY, 1996, pp. 267–278.

[27] J.K. Strauss-Soukup, L.J. Maher, DNA bending by GCN4 mutants bearing cationic residues, Biochemistry 36 (1997) 10026–10032.
[28] J. Strauss-Soukup, L. Maher, Electrostatic effects in DNA bending by GCN4 mutants, Biochemistry 37 (1998) 1060–1066.
[29] L.A. Tomky, J.K. Strauss-Soukup, L.J. Maher, Effects of phosphate neutralization on the shape of the AP-1 transcription factor binding site in duplex DNA, Nucleic Acids Res. 26 (1998) 2298–2305.
[30] G. Liang, L. Encell, M.G. Nelson, C. Switzer, D.E.G. Shuker, B. Gold, The role of electrostatics in the sequence selective reaction of charged alkylating agents with DNA, J. Am. Chem. Soc. 117 (1995) 10135–10136.
[31] P. Dande, G. Liang, F. Chen, C. Roberts, M.G. Nelson, H. Hashimoto, C. Switzer, B. Gold, Regioselective effect of zwitterionic DNA substitutions on DNA alkylation: evidence for a strong side chain orientational preference, Biochemistry 36 (1997) 6024–6032.
[32] H.S. Koo, J. Drak, J.A. Rice, D.M. Crothers, Determination of the extent of DNA bending by an adenine-thymine tract, Biochemistry 29 (1990) 4227–4234.
[33] D.M. Crothers, J. Drak, Global features of DNA structure by comparative gel electrophoresis, Methods Enzymol. 212 (1992) 46–71.
[34] E.D. Ross, R.B. Den, P.R. Hardwidge, L.J. Maher, Improved quantitation of DNA curvature using ligation ladders, Nucleic Acids Res. 27 (1999) 4135–4142.
[35] M. Ahmadian, P. Zhang, D.E. Bergstrom, A comparative study of the thermal stability of oligodeoxyribonucleotides containing 5-substituted 2′-deoxyuridines, Nucleic Acids Res. 26 (1998) 3127–3135.
[36] B.C. Froehler, R.J. Jones, X. Cao, T.J. Terhorst, Oligonucleotides derived from 5-(1-propynyl)-2′-*O*-allyl-uridine and 5-(1-propynyl)-2′-*O*-allyl-cytidine: synthesis and RNA duplex formation, Tetrahedron Lett. 34 (1993) 1003–1006.
[37] A.K. Phipps, M. Tarkoy, P. Schultze, J. Feigon, Solution structure of an intramolecular DNA triplex containing 5-(1-propynyl)-2′-deoxyuridine residues in the third strand, Biochemistry 37 (1998) 3820–3830.
[38] L.E. Heystek, H. Zhou, P. Dande, B. Gold, Control over the localization of positive charge in DNA: the effect on duplex DNA and RNA stability, J. Am. Chem. Soc. 120 (1998) 12165–12166.
[39] R.W. Wagner, M.D. Matteucci, J.G. Lewis, A.J. Gutierrez, C. Moulds, B.C. Froehler, Antisense gene inhibition by oligonucleotides containing C-5 propyne pyrimidines, Science 260 (1993) 1510–1513.
[40] M. Saunders, K.N. Houk, Y.D. Wu, W.C. Still, M. Lipton, G. Chang, W.C. Guida, Conformations of cycloheptadecane. A comparison of methods for conformational searching, J. Am. Chem. Soc. 112 (1990) 1419–1427.
[41] J.L. Sussman, E.N. Trifonov, Possibility of nonkinked packing of DNA in chromatin, Proc. Natl. Acad. Sci. USA 75 (1978) 103–107.
[42] H. Hashimoto, M.G. Nelson, C. Switzer, Formation of chimeric duplexes between zwitterionic and natural DNA, J. Org. Chem. 58 (1993) 4194–4195.
[43] H. Hashimoto, M.G. Nelson, C. Switzer, Zwitterionic DNA, J. Am. Chem. Soc. 115 (1993) 7128–7134.
[44] A.M. Gacy, C.T. McMurray, Influence of hairpins on template reannealing at trinucleotide repeat duplexes: a model for slipped DNA, Biochemistry 37 (1998) 9426–9434.
[45] S.J. Weiner, P.A. Kollman, D.T. Nguyen, D.A. Case, An all atom force field for simulations of proteins and nucleic acids, J. Comp. Chem. 7 (1986) 230–252.
[46] W.C. Still, A. Tempczyk, R.C. Hawley, T. Hendrickson, Semianalytical treatment of solvation for molecular mechanics and dynamics, J. Am. Chem. Soc. 112 (1990) 6127–6129.